

TIME PERIOD OF TAPERED PARALLELOGRAM SHAPED PLATE WITH EXPONENTIAL PROFILE IN YOUNG'S MODULUS


VREMENSKI PERIOD PLOČE OBLIKA SUŽENOG PARALELOGRAMA SA EKSPONENCIJALNIM PROFILOM JUNGVOG MODULA

Originalni naučni rad / Original scientific paper



Rad primljen / Paper received: 01.08.2023

<https://doi.org/10.69644/ivk-2024-03-0393>

Adresa autora / Author's address:

¹) Department of Mathematics, Amity School of Applied Sciences, Amity University Haryana, Gurugram, India N. Lather  0000-

0001-7896-844X; R. Bhardwaj  0000-003-2427-5108; A. Sharma  0000-003-4516-6955 **email: dba.amitsharma@gmail.com

²) Department of Mathematics, University Institute of Sciences, Chandigarh University, Chandigarh, Gharuan, Mohali, Punjab, India N. Mani  0000-0002-7131-2664; P. Ailawalia  0000-0003-4381-6299 *email: praveen_2117@rediffmail.com

Keywords

- density
- exponential
- skew plate
- Young's modulus
- time period

Abstract

The current study estimates the time period of frequency (four modes) of parallelogram shaped plate having circular density and thickness in one and two dimensions, in respect, along with exponential profile in Young's modulus for two different edge conditions. The two different edge conditions of the plate are CCSS and CSSS. The Rayleigh-Ritz method is implemented to solve the frequency equation for the system mentioned above. The major conclusion made from the study is that we can optimise the time period for the system by choosing the circular profile in density and thickness for such plates. To validate our findings, we compare our results with previously published data and show in tabular form.

INTRODUCTION

The study of vibration is universal due to its applications in applied science and engineering. Research on vibration of elastic plates with different plate parameters and boundary conditions has been done previously, but few have been done on nonuniform and nonhomogeneous parallelogram plates. Researchers are interested in finding out the vibration frequencies and other factors on such plates. This research focuses on the analysis of modes of frequency of nonhomogeneous plates with non-uniform thickness and Young's modulus. This analysis is important for understanding system performance/behaviour as engineering structures are made up of these plates. It is necessary to understand the characteristics of plate parameters efficiently in order to do such analysis.

Vibrational behaviour of a skew plate having variable thickness under temperature profile at clamped edges is described in /1/ using Rayleigh Ritz method and obtained the natural frequencies for the plates. Vibrational analysis of tapered functionally graded parallelogram plates are computed in /2/ and provided innovative results and effects of parameter on the frequency of the plates. A novel numerical approach is implemented in /3/ to study the vibrational behaviour of composite structures in quasi-static nonlinear

Ključne reči

- gustina
- eksponencijalna
- proizvodnja legura
- tribološka analiza
- površinsko oštećenje

Izvod

U radu se procenjuje vremenski period frekvencije (za četiri moda) ploče oblika paralelograma sa kružno raspodeljenom gustinom i debljinom u jednoj i dve dimenzije, respektivno, ujedno i sa eksponencijalnim profilom Jungovog modula za dva različita granična uslova ivica. Dva različita uslova ivica ploče su CCSS i CSSS. Primenjen je Rejlej-Ricov metod za rešavanje frekventnog izraza za gore spomenuti sistem. Glavni zaključak koji se izvodi u radu je da se za ovakve ploče može optimizovati vremenski period sistema izborom kružnog profila po gustini i debljini. Kako bismo verifikovali naše rezultate, upoređujemo ih sa objavljenim podacima i predstavljamo ih u tabelarnom obliku.

equilibrium states and a hybrid quasi three-dimensional theory for stresses, deflections, and vibrational analysis of bi-functionally graded sandwich plates resting on Pasternak's elastic foundations is established in /4/. Peng et al. /5/ proposed geometric nonlinear analysis of arbitrary polygonal and circular stiffened plates by using meshless Galerkin method based on the first-order shear deformation theory and a series of points were used to discretize the flat plate and stiffeners to achieve the meshless model of stiffened plates. Bera et al. /6/ investigated the transverse vibrations of square/rectangular (isotropic and orthotropic) plates using the Navier method to obtain vibrational frequencies and mode shapes for the plates, as well as the best suitable plate thickness range for CLPT and HSDT models for improved buckling load calculation accuracy. Lee and Lim /7/ calculated the vibrational behaviour of square (isotropic and orthotropic) plates with square cutouts subjected to in-plane forces and all frequency parameters were obtained by Rayleigh-Ritz method. Impact of temperature on square plates was observed by Kumar et al. /8/ for clamped and simply supported. Authors calculated the modes of frequency by using Rayleigh-Ritz technique and reduce the frequency of the plate with different plate parameters. In this series, Kaur /9/ also worked on effect of temperature for clamped triangular plate by employing Rayleigh-Ritz technique to solve

the frequency equation (first two modes) for the system with respect to different values of temperature, thickness and aspect ratios. In 2017, Sharma /10/ dealt with vibrational frequencies of square plate for various geometrical and thermal conditions and demonstrated the impact of tapering along with bilinear temperature. Liu et al. /11/ introduced a novel semi-analytical dynamic model and a new nonlinear mechanical bolted joint model to analyse the vibrational behaviours of mistuning bolted composite plates and revealed the cause of the mistuning bolted structure's nonlinear phenomena. Vibrational behaviours of cylindrical functionally graded porous (FGP) panels and shells are examined in /12/. FSDT and Hamilton's principle are used to determine the weak form for free vibration of FGP shells. In order to tackle the issue, the isogeometric analysis (IGA) approach is used, and NURBS is used to create a geometric model and define the displacement fields.

The main aim of the study is to show the impact of thickness and density of circular profile in two and one dimension respectively along with exponential Young's modulus at CCSS and CSSS boundary conditions on time period of parallelogram shaped plate. For validating the key results achieved in this study, authors did comparisons with already cited results in literature in terms of frequency modes of the studied plate.

ANALYSIS

Consider a nonhomogeneous parallelogram plate with skew angle θ and skew coordinates $\zeta = x - y \tan \theta$, $\psi = y \sec \theta$.

The relation for kinetic T_s and strain energy V_s is expressed as mentioned in /13/,

$$T_s = \frac{1}{2} \omega^2 \cos \theta \iint_R \rho l \Phi^2 d\zeta d\psi, \quad (1)$$

$$V_s = \frac{1}{2 \cos^3 \theta} \iint_R D_1 \left[\left(\frac{\partial^2 \Phi}{\partial \zeta^2} \right)^2 - 4 \sin \theta \left(\frac{\partial^2 \Phi}{\partial \zeta^2} \right) \left(\frac{\partial^2 \Phi}{\partial \zeta \partial \psi} \right) + 2(\sin^2 \theta + \nu \cos^2 \theta) \left(\frac{\partial^2 \Phi}{\partial \zeta^2} \right) \left(\frac{\partial^2 \Phi}{\partial \psi^2} \right) + 2(1 + \sin^2 \theta - \nu \cos^2 \theta) \left(\frac{\partial^2 \Phi}{\partial \zeta \partial \psi} \right)^2 - 4 \sin \theta \left(\frac{\partial^2 \Phi}{\partial \zeta \partial \psi} \right) \left(\frac{\partial^2 \Phi}{\partial \psi^2} \right) + \left(\frac{\partial^2 \Phi}{\partial \psi^2} \right)^2 \right] d\zeta d\psi. \quad (2)$$

Here, l , ρ , ν , ω , and Φ represent thickness, density, Poisson's ratio, natural frequency, deflection function, respectively, and $D_1 = E l^3 / 12(1 - \nu^2)$ is known as flexural rigidity.

Rayleigh-Ritz method imposes that maximal value of strain energy must be equal to maximal value of kinetic energy,

$$I = \delta(V_s - T_s) = 0. \quad (3)$$

Substituting Eqs. (1) and (2) in Eq.(3),

$$I = \frac{1}{2 \cos^3 \theta} \iint_R D_1 \left[\left(\frac{\partial^2 \Phi}{\partial \zeta^2} \right)^2 - 4 \sin \theta \left(\frac{\partial^2 \Phi}{\partial \zeta^2} \right) \left(\frac{\partial^2 \Phi}{\partial \zeta \partial \psi} \right) + 2(\sin^2 \theta + \nu \cos^2 \theta) \left(\frac{\partial^2 \Phi}{\partial \zeta^2} \right) \left(\frac{\partial^2 \Phi}{\partial \psi^2} \right) + 2(1 + \sin^2 \theta - \nu \cos^2 \theta) \left(\frac{\partial^2 \Phi}{\partial \zeta \partial \psi} \right)^2 - 4 \sin \theta \left(\frac{\partial^2 \Phi}{\partial \zeta \partial \psi} \right) \left(\frac{\partial^2 \Phi}{\partial \psi^2} \right) + \left(\frac{\partial^2 \Phi}{\partial \psi^2} \right)^2 \right] - \frac{1}{2} \omega^2 \cos \theta \iint_R \rho l \Phi^2 d\zeta d\psi = 0. \quad (4)$$

Now introducing two-dimensional circular thickness (refer Fig. 2), one-dimensional circular density is taken expressed as in /14/, and one-dimensional exponential variation in Young's modulus is taken as

$$l = l_0 \left[1 + \beta_1 \left(1 - \sqrt{1 - \frac{\zeta^2}{a^2}} \right) \right] \left[1 + \beta_2 \left(1 - \sqrt{1 - \frac{\psi^2}{b^2}} \right) \right], \quad \rho = \rho_0 \left[1 - m \left(1 - \sqrt{1 - \frac{\zeta^2}{a^2}} \right) \right], \quad E = E_0 e^{\frac{m_1 \zeta}{a}}, \quad (5)$$

where: l_0 , E_0 , and ρ_0 are the thickness, Young's modulus, and density at origin; β_1 , β_2 are tapering parameters; and m_1 , m are nonhomogeneity parameters.

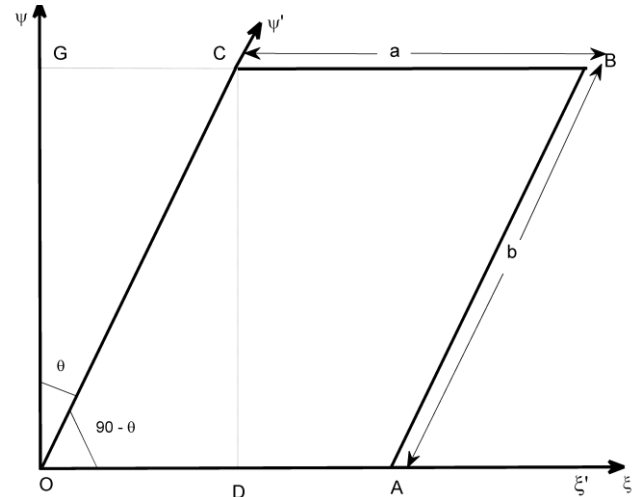


Figure 1. Parallelogram plate with skew angle θ .

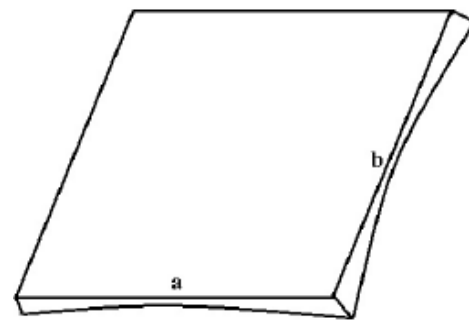


Figure 2. Parallelogram-shaped plate with thickness of circular (two-dimensional) profile.

Using Eq.(5), Eq.(4) becomes

$$I = \frac{D_0}{2} \int_0^a \int_0^b [1 + \beta_1 \Psi_1]^3 [1 + \beta_2 \Psi_2]^3 e^{m_1 \frac{\zeta}{a}} \left[\left(\frac{\partial^2 \Phi}{\partial \zeta^2} \right)^2 - 4 \left(\frac{a}{b} \right) \sin \theta \left(\frac{\partial^2 \Phi}{\partial \zeta^2} \right) \left(\frac{\partial^2 \Phi}{\partial \zeta \partial \psi} \right) + 2 \left(\frac{a}{b} \right)^2 (\sin^2 \theta + \nu \cos^2 \theta) \left(\frac{\partial^2 \Phi}{\partial \zeta^2} \right) \left(\frac{\partial^2 \Phi}{\partial \psi^2} \right) + 2 \left(\frac{a}{b} \right)^2 (1 + \sin^2 \theta - \nu \cos^2 \theta) \left(\frac{\partial^2 \Phi}{\partial \zeta \partial \psi} \right)^2 - 4 \left(\frac{a}{b} \right)^3 \sin \theta \left(\frac{\partial^2 \Phi}{\partial \zeta \partial \psi} \right) \left(\frac{\partial^2 \Phi}{\partial \psi^2} \right) + \left(\frac{a}{b} \right)^4 \left(\frac{\partial^2 \Phi}{\partial \psi^2} \right)^2 \right] d\psi d\zeta - \lambda^2 \cos^4 \theta \int_0^a \int_0^b [1 + \beta_1 \Psi_1][1 + \beta_2 \Psi_2][1 - m \Psi_1] \Phi^2 d\psi d\zeta = 0, \quad (6)$$

$$\text{where: } \Psi_1 = \left(1 - \sqrt{1 - \frac{\zeta^2}{a^2}} \right); \Psi_2 = \left(1 - \sqrt{1 - \frac{\psi^2}{b^2}} \right); D_0 = \frac{E_0 l_0^3}{12(1 - \nu^2)}; \lambda^2 = \frac{\rho_0 \omega^2 l_0 a^4}{D_0}.$$

The two-term deflection function is taken as in [16],

$$\Phi(\zeta, \psi) = \left[\left(\frac{\zeta}{a} \right)^p \left(\frac{\psi}{b} \right)^q \left(1 - \frac{\zeta}{a} \right)^r \left(1 - \frac{\psi}{b} \right)^s \right] \left[\sum_{i=0}^n \Omega_i \left\{ \left(\frac{\zeta}{a} \right) \left(\frac{\psi}{b} \right) \left(1 - \frac{\zeta}{a} \right) \left(1 - \frac{\psi}{b} \right) \right\}^i \right]. \quad (7)$$

In Eq.(7) the values of variables $p, q, r,$ and s depend on boundary conditions. The variables will have values 0, 1, 2 if the edge conditions were free, simply supported, and clamped, respectively. The arbitrary constants $\Omega_i, i = 0, 1, 2, \dots, N$ signify the number of frequency modes.

For minimising the functional mentioned in Eq.(6), the following constraints need to be satisfied:

$$\frac{\partial I}{\partial \Omega_i} = 0, \quad i = 0, 1, 2, \dots, n. \quad (8)$$

On solving Eq.(8), we obtain the desired frequency equation as:

$$|P - \lambda^2 Q| = 0, \quad (9)$$

where: $P = [p_{ij}]_{n+1}, Q = [q_{ij}]_{n+1}$, are square matrices; and $i, j = 0, 2, 2, \dots, n$.

Equation (10) mentioned below is used for computing the time period for frequency λ obtained from Eq.(9),

$$K = \frac{2\pi}{\lambda}. \quad (10)$$

NUMERICAL WORK AND DISCUSSION

Here, authors report the obtained results for the parallelogram plate (for first four modes) with the configuration: two-dimensional circular thickness, one-dimensional circular density and one-dimensional exponential Young's modulus variations. The parameters which we are kept fixed in this study are aspect ratio $a/b = 1.5$ (refer to Fig. 2), skew angle $\theta = 30^\circ$ and Poisson's ratio $\nu = 0.345$.

Table 1 describes the obtained time period K at CCSS and CSSS edge conditions corresponding to nonhomogeneity parameter m_1 . In this table, the time period is evaluated for two different set values of tapering parameters β_1, β_2 , and nonhomogeneity parameter m (due to variation in density ρ), i.e., Set I: $\beta_1 = \beta_2 = m = -0.3$; Set II: $\beta_1 = \beta_2 = m = 0.3$:

- the nonhomogeneity parameter m_1 is varied from -0.3 to 0.3 . The below conclusions are made from Table 1.
- The time period decreases with the increasing value of nonhomogeneity parameter m_1 for the above mentioned edge conditions.
- The time period obtained at CCSS is less as compared to the CSSS edge condition, but the decremental rate of time period achieved at CSSS is less (1.56 %) as compared to the CCSS edge condition.

Also here, the time period decreases at the above mentioned edge conditions, when we move from Set I to Set II.

Table 2 demonstrates the time period K at CCSS and CSSS boundary conditions for nonhomogeneity parameter m . In this table, the nonhomogeneity parameter m_1 and two distinct sets of tapering parameters β_1, β_2 are examined over the time period.

Set III: $\beta_1 = \beta_2 = m_1 = -0.3$; Set IV: $\beta_1 = \beta_2 = m_1 = 0.3$. The nonhomogeneity parameter m ranges from -0.3 to 0.3 .

The facts observed in Table 2 are as follows:

- the time period also decreases with increasing value of nonhomogeneity parameter m for the above mentioned edge conditions. But the decremental rate in time period presented in Table 2 is less as compared to the time period presented in Table 1. This aspect is due to choosing circular variation in density parameter;
- the time period achieved at CCSS is also less (as like in Table 1) as compared to CSSS boundary condition, but the decremental rate in time period achieved at CSSS is high (2.29 %) as compared to CCSS edge condition;
- as like in Table 1, here also, the time period decreases at the above mentioned edge conditions, when we move from Set III to Set IV.

Table 3 demonstrates the parallelogram time period K at CCSS and CSSS edge conditions for nonhomogeneity parameter m . In this table, the nonhomogeneity parameter m_1 and two distinct sets of tapering parameters (β_1, β_2) are examined over the time period.

Set V: $m = m_1 = -0.3$; Set VI: $m = m_1 = 0.3$. The tapering parameters (β_1, β_2) range from -0.3 to 0.3 . From Table 3, one can conclude that:

- the time period K also decreases with increasing value of tapering parameters for above mentioned edge conditions;
- as like in Tables 1 and 2, here also, the time period achieved at CCSS is also less (as like in Tables 1, 2) as compared to CSSS boundary condition, but decremental rate in time period achieved at CSSS was high (2.29 %) as compared to the CCSS edge condition;
- as in Tables 1, 2, here also, the time period decreases at the above mentioned edge conditions, when we move from Set V to Set VI.

Table 1. Time period of skew plate at CCSS and CSSS edge conditions corresponding to nonhomogeneity m_1 .

CCSS								
m_1	Set I: $\beta_1 = \beta_2 = m = -0.3$				Set II: $\beta_1 = \beta_2 = m = 0.3$			
	K_1	K_2	K_3	K_4	K_1	K_2	K_3	K_4
-0.3	0.120272	0.031067	0.012741	0.002884	0.108780	0.028781	0.011556	0.002474
-0.1	0.112700	0.029357	0.012043	0.002715	0.101775	0.027180	0.010913	0.002326
0.1	0.105546	0.027730	0.011379	0.002555	0.095170	0.025659	0.010301	0.002187
0.3	0.098790	0.026183	0.010746	0.002403	0.088948	0.024213	0.0097192	0.002055
CSSS								
-0.3	0.176367	0.034101	0.013548	0.003326	0.159848	0.031905	0.012615	0.002993
-0.1	0.165504	0.032202	0.012788	0.003129	0.149601	0.030106	0.011897	0.002812
0.1	0.155183	0.030397	0.012065	0.002942	0.139901	0.028397	0.011215	0.002640
0.3	0.145391	0.028682	0.011378	0.002764	0.130733	0.026774	0.010567	0.002477

Table 2. Time period of skew plate at CCSS and CSSS edge conditions corresponding to nonhomogeneity m .

CCSS								
m	Set III: $\beta_1 = \beta_2 = m_1 = -0.3$				Set IV: $\beta_1 = \beta_2 = m_1 = 0.3$			
	K_1	K_2	K_3	K_4	K_1	K_2	K_3	K_4
-0.3	0.120272	0.031067	0.012741	0.002884	0.095346	0.026175	0.010644	0.002314
-0.1	0.117702	0.030323	0.012397	0.002784	0.093261	0.025542	0.010347	0.002231
0.1	0.115075	0.029555	0.012039	0.002678	0.091129	0.024889	0.010040	0.002145
0.3	0.112389	0.028762	0.011666	0.002567	0.088948	0.024213	0.009719	0.002055
CSSS								
-0.3	0.176367	0.034101	0.013548	0.003326	0.140468	0.029059	0.011591	0.002804
-0.1	0.172512	0.033255	0.013177	0.003207	0.137298	0.028323	0.011264	0.002700
0.1	0.168570	0.032381	0.012791	0.003081	0.134055	0.027563	0.010923	0.002592
0.3	0.164535	0.031477	0.012388	0.002950	0.130733	0.026774	0.010567	0.002477

Table 3. Time period of skew plate at CCSS and CSSS edge conditions corresponding to tapering parameters β_1, β_2 .

CCSS								
$\beta_1 = \beta_2$	Set V: $m_1 = m = -0.3$				Set VI: $m_1 = m = 0.3$			
	K_1	K_2	K_3	K_4	K_1	K_2	K_3	K_4
-0.3	0.120272	0.031067	0.012741	0.002884	0.092342	0.024243	0.009836	0.002138
-0.1	0.118913	0.031086	0.012705	0.002841	0.091067	0.024233	0.009791	0.002103
0.1	0.117714	0.031102	0.012676	0.002810	0.089944	0.024223	0.009752	0.002076
0.3	0.116647	0.031115	0.012651	0.002785	0.088948	0.024213	0.009719	0.0020551
CSSS								
-0.3	0.176367	0.034101	0.013548	0.003326	0.135666	0.026481	0.010400	0.002451
-0.1	0.174770	0.034307	0.013657	0.003352	0.133897	0.026595	0.010465	0.002463
0.1	0.173247	0.034483	0.013751	0.003371	0.132256	0.026692	0.010520	0.002471
0.3	0.171803	0.034634	0.013832	0.003387	0.130733	0.026774	0.010567	0.002477

COMPARISON OF RESULTS

In this section, authors did a comparison of vibrational frequency modes (for first four modes) achieved in current research and achieved in /15/ with respect to m for fixed value of tapering parameters β_1, β_2 , Young's modulus m_1 , and angle of skewness θ (i.e., $\beta_1 = \beta_2 = m_1 = 0.0$ and $\theta = 30^\circ$). In Fig. 3, authors compare nonhomogeneity in which the present study deals with circular nonhomogeneity and /15/ deals with exponential nonhomogeneity.

From Fig. 3, we conclude that:

- frequency modes obtained in current research increase, while modes of frequency obtained in /15/ decrease, when nonhomogeneity parameter varies from 0.0 to 0.9;
- rates of change of frequencies obtained in present study are slower as compared to frequencies obtained in /15/.

CONCLUSIONS

In this study, authors show the impact of two-dimensional circular variation in thickness, one-dimensional circu-

lar variation in density and Young's modulus on time period K and frequency modes λ and of parallelogram-shaped plate at CCSS and CSSS edge conditions. From the comparison of results and numerical results discussions, authors conclude the following facts:

- circular variation in density provides the less time period of modes of vibration (present study) in comparison to exponential variation in density /15/ at CCCC edge condition (refer to Fig. 3);
- variation in both nonhomogeneity parameters m, m_1 results in decreased time period at CCSS and CSSS edge conditions (refer to Tables 1 and 2);
- circular variation in density provides less variation in time period as compared to exponential variation in Young's modulus;
- variation in parameters β_1, β_2 results in decreased time period at CCSS and CSSS edge conditions (refer to Table 3).

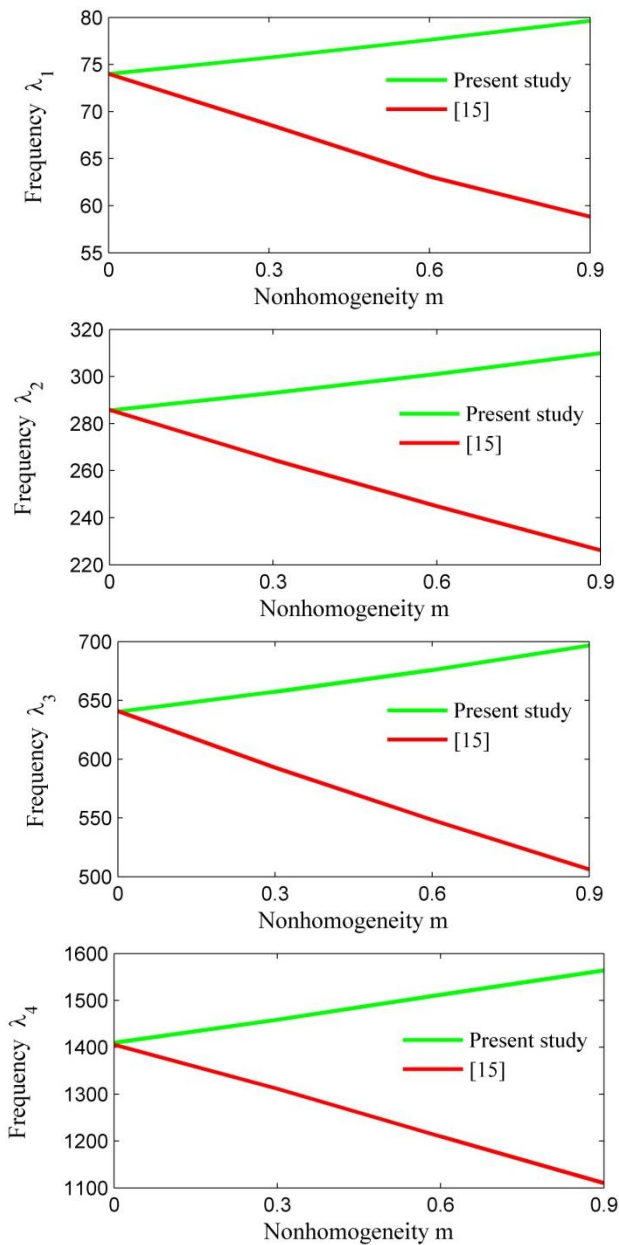


Figure 3. Comparison of frequency modes achieved in current research and achieved in [15] corresponding to nonhomogeneity m .

REFERENCES

- Bhardwaj, R., Mani, N. (2019), *Modelling on vibration of skew plate with thickness and temperature variation*, Vibroeng. Procedia, 22: 6-12. doi: 10.21595/vp.2019.20544
- Chen, M., Ye, T., Zhang, J., et al. (2020), *Isogeometric three-dimensional vibration of variable thickness parallelogram plates with in-plane functionally graded porous materials*, Int. J Mech. Sci. 169: 105304. doi: 10.1016/j.ijmecsci.2019.105304
- Pagani, A., Azzara, R., Carrera, E. (2023), *Geometrically nonlinear analysis and vibration of in-plane-loaded variable angle tow composite plates and shells*, Acta Mech. 234(1): 85-108. doi: 10.1007/s00707-022-03226-2
- Van Vinh, P. (2023), *Deflections stresses and free vibration analysis of bi-functionally graded sandwich plates resting on Pasternak's elastic foundations via a hybrid quasi-3D theory*, Mech. Based Des. Struct. Mach. 51(4): 2323-2354. doi: 10.1080/15397734.2021.1894948

- Peng, L.X., Xiang, J., Qin, X., et al. (2023), *A meshless method for geometric nonlinear analysis of arbitrary polygonal and circular stiffened plates*, Int. J Non-Linear Mech. 148: 104233. doi: 10.1016/j.ijnonlinmec.2022.104233
- Bera, P., Varun, J.P., Mahato, P.K. (2022), *Buckling analysis of isotropic and orthotropic square/rectangular plate using CLPT and different HSDT models*, Mater. Today: Proc. 56(Part 1): 237-244. doi: 10.1016/j.matpr.2022.01.106
- Lee, H.P., Lim, S.P. (1992), *Free vibration of isotropic and orthotropic square plates with square cutouts subjected to in-plane forces*, Comput. Struct. 43(3): 431-437. doi: 10.1016/0045-7949(92)90276-6
- Kumar, A., Lather, N., Sharma, A. (2019), *Analysis of time period of isotropic square plate on clamped and simply supported conditions*, AIP Conf. Proc. 2142(1): 110026. doi: 10.1063/1.5122486
- Kaur, N. (2020), *Vibrational behavior of tapered triangular plate with clamped ends under thermal condition*, J Inst. Eng. (India): Ser. C, 101(2): 391-399. doi: 10.1007/s40032-019-00551-9
- Sharma, A. (2017), *Vibration of square plate with parabolic temperature variation*, Rom. J Acoust. Vibr. 14(2): 107-114.
- Liu, H., Sun, W., Du, D., et al. (2023), *Nonlinear vibration of mistuning bolted composite plates considering stick-slip-separation characteristics*, Int. J Mech. Sci. 245: 108126. doi: 10.1016/j.ijmecsci.2023.108126
- Xue, Y., Jin, G., Zhang, C., et al. (2023), *Free vibration analysis of functionally graded porous cylindrical panels and shells with porosity distributions along the thickness and length directions*, Thin-Wall. Struct. 184: 110448. doi: 10.1016/j.tws.2022.110448
- Chakraverty, S., *Vibration of Plates*, 1st Ed., CRC Press, Boca Raton, 2008. doi: 10.1201/9781420053968
- Lather, N., Bhardwaj, R., Sharma, A., Kumar, K. (2022), *Time period analysis of orthotropic skew plate with 2-D circular thickness and 1-D circular density*, Math. Probl. Eng. 2022: Art. ID 7880806. doi: 10.1155/2022/7880806
- Bhardwaj, R., Mani, N. (2021), *Vibration of skew plate having exponential variation in Young's modulus and density*, J Theor. Appl. Mech. 51(1): 92-102.
- Sharma, A., Bhardwaj, R., Lather, N., et al. (2022), *Time period of thermal-induced vibration of skew plate with two-dimensional circular thickness*, Math. Probl. Eng. 2022(1): Art. ID 8368194. doi: 10.1155/2022/8368194

© 2024 The Author. Structural Integrity and Life, Published by DIVK (The Society for Structural Integrity and Life 'Prof. Dr Stojan Sedmak') (<http://divk.inovacionicentar.rs/ivk/home.html>). This is an open access article distributed under the terms and conditions of the Creative Commons Attribution-NonCommercial-NoDerivatives 4.0 International License